An outburst from a massive star 40 days before a supernova explosion

E. O. Ofek[1], M. Sullivan[2,3], S. B. Cenko[4], M. M. Kasliwal[5], A. Gal-Yam[1], S. R. Kulkarni[6], I. Arcavi[1], L. Bildsten[7,8], J. S. Bloom[4,9], A. Horesh[6], D. A. Howell[8,10], A. V. Filippenko[4], R. Laher[11], D. Murray[12], E. Nakar[13], P. E. Nugent[9,4], J. M. Silverman[4,14], N. J. Shaviv[15], J. Surace[11], O. Yaron[1]

[1] Benoziyo Center for Astrophysics, Weizmann Institute of Science, 76100 Rehovot, Israel.

[2] School of Physics and Astronomy, University of Southampton, Southampton, SO17 1BJ, UK.

[3] Department of Physics (Astrophysics), University of Oxford, Keble Road, Oxford, OX1 3RH, UK.

[4] Department of Astronomy, University of California, Berkeley, CA 94720-3411, USA.

[5] Observatories of the Carnegie Institution for Science, 813 Santa Barbara St., Pasadena, CA 91101, USA.

[6] Division of Physics, Mathematics, and Astronomy, California Institute of Technology, Pasadena, CA 91125, USA.

[7] Kavli Institute for Theoretical Physics, Kohn Hall, University of California, Santa Barbara, CA 93106, USA.

[8] Department of Physics, Broida Hall, University of California, Santa Barbara, CA 93106, USA.

[9] Lawrence Berkeley National Laboratory, 1 Cyclotron Road, Berkeley, CA 94720, USA.

[10] Las Cumbres Observatory Global Telescope Network, 6740 Cortona Dr., Suite 102, Goleta, CA 93117, USA.

[11] Spitzer Science Center, California Institute of Technology, M/S 314-6, Pasadena, CA 91125, USA.

[12] Physics Department, University of Wisconsin–Milwaukee, Milwaukee, WI 53211, USA.

[13] School of Physics and Astronomy, Tel-Aviv University, Tel-Aviv, Israel.

[14] Department of Astronomy, University of Texas, Austin, TX 78712-0259, USA.

[15] Racah Institute of Physics, The Hebrew University, 91904 Jerusalem, Israel.

Various lines of evidence suggest that very massive stars experience extreme mass-loss episodes shortly before they explode as a supernova.[1−4] Interestingly, several models predict such pre-explosion outbursts.[5−7] Establishing a causal connection between these mass-loss episodes and the final supernova explosion will provide a novel way to study pre-supernova massive-star evolution. Here we report on observations of a remarkable mass-loss event detected 40 days prior to the explosion of the Type IIn supernova SN 2010mc (PTF 10tel). Our photometric and spectroscopic data suggest that this event is a result of an energetic outburst, radiating at least 6×10^{47} erg of energy, and releasing about

$10^{-2}\,M_\odot$ at typical velocities of 2000 km s^{-1}. We show that the temporal proximity of the mass-loss outburst and the supernova explosion implies a causal connection between them. Moreover, we find that the outburst luminosity and velocity are consistent with the predictions of the wave-driven pulsation model[6], and disfavour alternative suggestions[7].

Type IIn supernovae (SNe IIn) are a diverse class of transient events, spectroscopically defined by narrow and/or intermediate-width hydrogen emission lines, up to a few thousand km s^{-1} in width.[8–10] These emission lines likely originate from optically thin circumstellar matter excited by the SN shock and/or radiation field. The spectra and light curves of these SNe are interpreted as signatures of interaction between the SN ejecta and mass that has been expelled prior to the explosion.[11–13] The best case in which the progenitor of a SN IIn has been detected prior to the SN explosion[3] was likely a luminous blue variable (LBV) – a class of objects which are known for their vigorous eruptive mass-loss events[14]. Very recently, a massive star in the nearby galaxy NGC 7259, SN 2009ip, had a series of outbursts[15–17] with a typical velocity of about 500 km s^{-1}, possibly followed by an ongoing supernova event[18–19] exhibiting P-Cygni lines with velocities of $\sim 10^4$ km s^{-1}. Another possibly related event is SN 2006jc that is further discussed in SI §7.

The Palomar Transient Factory[20–21] discovered the Type IIn SN 2010mc (PTF 10tel)[24] in images obtained on 2010 Aug. 20.22 (UTC dates are used throughout this paper). It is located at $\alpha = 17^{\rm h}21^{\rm m}30.^{\rm s}68$, $\delta = +48°07'47.''4$ (J2000.0), at redshift $z = 0.035$ which corresponds to a luminosity distance of 153 Mpc. Our ongoing search for precursor events in pre-explosion images of nearby PTF SNe IIn revealed a positive detection at the SN location in images taken prior to the SN discovery (Figure 1). Here we measure time relative to 2010 Aug. 20.22, which corresponds to the onset of the SN explosion (main event; Fig. 1). The initial bump emerged at day −37 relative to the SN discovery date, and peaked at an absolute magnitude of about −15 ($\sim 2.25\times10^{41}$ erg s^{-1}) in the $R_{\rm PTF}$ band. The main SN explosion then brightened for two weeks and peaked at an $R_{\rm PTF}$ absolute magnitude of −18.4 ($\sim 5.2\times10^{42}$ erg s^{-1}), radiating a total bolometric luminosity of $\sim 3\times10^{49}$ erg, while the precursor bump radiated $\sim 6\times10^{47}$ erg (or more due to the unknown bolometric correction).

Spectra of the supernova, showing a blue continuum with Balmer emission lines, are presented in Figure 2. The continuum becomes redder with time, and its slope corresponds to an effective temperature of over 16,000 K at day five and drops to about 8,000 K at day 27. The Hα line has an initial width of $\sim 3\times10^3\,\mathrm{km\,s^{-1}}$ at day 6, decreasing to $\sim 10^3\,\mathrm{km\,s^{-1}}$ at day 14. A broad ($10^4\,\mathrm{km\,s^{-1}}$) P-Cygni profile emerges by day 27. The spectra also show He I lines with decreasing strength, presumably due to the drop in temperature.

The nature of the precursor bump is very intriguing and can potentially tell us a great deal about the SN explosion and the progenitor. The only interpretation that is fully consistent with the photometric and spectroscopic evidence is that the first bump represents an outburst from the SN progenitor about one month prior to explosion, while the brighter bump is initiated by a full explosion of the star a few weeks later. Below we analyse this model in the context of the photometric and spectroscopic data. In SI §6 we discuss some alternative models and conclude that they are unlikely.

The mass ejected by the precursor burst can be estimated in various independent ways. By requiring that the precursor integrated bolometric luminosity, $E_{\rm bol,prec}$, is lower than the kinetic energy of the precursor outburst (moving at velocity $v_{\rm prec}$) which powers it, we can set a lower limit on the mass ejected in the precursor outburst $M_{\rm prec} \gtrsim 2E_{\rm bol,prec}v_{\rm prec}^{-2} \approx 1.5\times10^{-2}(v_{\rm prec}/2000\,\mathrm{km\,s^{-1}})^{-2}\,\mathrm{M_\odot}$. The outburst velocity is estimated from the line widths of 1000–3000 $\mathrm{km\,s^{-1}}$, seen in the early-time spectra of the SN. As this mass was presumably ejected over a period of about one month (i.e., the outburst duration), the annual mass-loss rate is about 10 times higher. A similar order of magnitude argument can be used to put an upper limit on the mass in the precursor outburst. If some of the SN bolometric energy, $E_{\rm bol,SN}$, is due to interaction between the SN ejecta, moving at $v_{\rm SN}$, and the precursor shell, and assuming high efficiency of conversion of the kinetic energy to luminosity, then $M_{\rm prec} \lesssim 2E_{\rm bol,SN}v_{\rm SN}^{-2} \approx 3\times10^{-2}(v_{\rm SN}/10^4\,\mathrm{km\,s^{-1}})^{-2}\,\mathrm{M_\odot}$.

Another method to estimate the mass in the ejecta is based on the Hα emission-line luminosity and the radius of the photosphere, which is determined from a black-body fit to the spectra (SI Fig. 2). This method, derived in SI §2, suggests a mass-loss rate of $\gtrsim 10^{-1}\,\mathrm{M_\odot\,yr^{-1}}$, or a total ejected mass of $\gtrsim 10^{-2}\,\mathrm{M_\odot}$, if we assume a month-long outburst with a mean wind velocity of $2000\,\mathrm{km\,s^{-1}}$.

Another independent method for estimating the mass in the CSM is based on the rise time of the supernova. Since photons diffuse through material between the SN and the observer, the SN rise time gives us an upper limit on the diffusion time scale and therefore the total intervening mass. Since the SN rise time was about one week, this argument suggests that if the shell is spherically symmetric its total mass cannot exceed about $0.4\,M_\odot$ (see SI §5). Therefore, the kinetic-energy arguments, the Hα luminosity, the diffusion time scale, and the X-ray limits (see SI §3) are consistent with each other and indicate that the total mass lost during the outburst is of order $\sim 10^{-2}\,M_\odot$.

Our model for the sequence of events is presented in Figure 3. In a nutshell, this model suggests that the precursor outburst ejected $\sim 10^{-2}\,M_\odot$ at a velocity of $2000\,km\,s^{-1}$ about one month prior to the SN explosion. Shortly after the SN explosion, this ejected material was engulfed by the SN ejecta. At later times, after the optical depth decreases, we start seeing indications for the high velocity of the SN ejecta. We discuss some less likely alternative models in the SI §6.

A surprising result is the short time between the outburst and the explosion, which is a tiny fraction ($\sim 10^{-8}$) of the lifetime of a massive star. Even if massive stars have multiple mass-loss episodes (with mass loss $\gtrsim 10^{-2}\,M_\odot$) during their lifetime, the number of such episodes cannot exceed ~ 5000; otherwise, it will exceed a typical stellar mass. A conservative estimate shows that so far it might be possible to detect such an outburst in a sample of up to about 20 nearby SNe IIn, which have deep pre-explosion observations (see SI §7). Therefore, the probability of observing a random burst one month prior to the explosion is 0.1%. We conclude that such outbursts are either causally related to, or at least two orders of magnitude more common before, the final stellar explosion.

When considering where such an eruption could originate, one is led to the stellar core, as the binding energy it can liberate by contraction and nuclear reactions is sufficiently large. Because the actual luminosity is most likely neutrino-dominated, the Kelvin-Helmholtz time scale for this contraction can be short enough to explain the precursor's rapid rise in luminosity. However, the energy liberated at the core must reach the envelope, and it therefore requires a fast and efficient mechanism[6]. There are several proposed mechanisms that predict high mass-loss rates prior to the final stellar explosion. Recently,

it was suggested[6] that in some massive stars the super-Eddington fusion luminosities, shortly prior to core collapse, can drive convective motions that in turn excite gravity waves that propagate toward the stellar surface. The dissipation of these waves can unbind up to several solar masses of the stellar envelope. Alternatively, it was suggested[7] that the mass loss is driven by a common-envelope phase[25] due to the inspiral of a neutron star into a giant companion core (a so-called Thorne-Żytkow object), unbinding the companion envelope and setting up accretion onto the neutron star that collapses into a black hole and triggers a SN explosion shortly thereafter. This model, however, predicts an outflow velocity that is considerably lower than the one observed in the precursor of SN 2010mc, and is therefore disfavoured. Another possible mechanism is the pulsational pair instability SN[26]. However, current models predict that the mass ejected in these events will likely be much larger than the $10^{-2}\,M_{\odot}$ seen in SN 2010mc for the observed 40 day delay between the two last explosions.[5],[27]

The velocity and energetics of the precursor of SN 2010mc are consistent with the predictions of the wave-driven outburst mechanism[6]. However, a more detailed theoretical investigation is required in order to test that this model is consistent with all the observational evidence. Moreover, in SI §8, given the observed precursor luminosity, we theoretically derive the mass loss to be $\sim 0.05\,M_{\odot}$, in excellent agreement with our mass-loss estimates. Furthermore, we note that the velocity of the precursor ejecta is higher than predicted by other models.[7] Finally, we note that the mass-loss velocity in SN 2010mc is considerably higher than the one observed in SN 2009ip,[18] although the mass-loss rate was similar.[28]

Received 13 February 2013; Accepted **draft**.

1. Dopita, M. A., Cohen, M., Schwartz, R. D., & Evans, R., The 1984 supernova in NGC 3169 — Evidence for a superwind. *Astrophys. J.*, **287**, L69-L71 (1984)

2. Chugai, N. N., & Danziger, I. J., Supernova 1988Z — Low-Mass Ejecta Colliding with the Clumpy Wind. *Mon. Not. R. Astron. Soc.*, **268**, 173-180 (1994)

3. Gal-Yam, A., & Leonard, D. C., A massive hypergiant star as the progenitor of the supernova SN 2005gl. *Nature*, **458**, 865-867 (2009)

4. Ofek, E. O., Rabinak, I., Neill, J. D., et al., Supernova PTF 09UJ: A Possible Shock Breakout from a Dense Circumstellar Wind. *Astrophys. J.*, **724**, 1396-1401 (2010)

5. Woosley, S. E., Blinnikov, S., & Heger, A., Pulsational pair instability as an explanation for the most luminous supernovae. *Nature*, **450**, 390-392 (2007)

6. Quataert, E., & Shiode, J., Wave-driven mass loss in the last year of stellar evolution: setting the stage for the most luminous core-collapse supernovae. *Mon. Not. R. Astron. Soc.*, **423**, L92-L96 (2012)

7. Chevalier, R. A., Common Envelope Evolution Leading to Supernovae with Dense Interaction. *Astrophys. J. Letters*, **752**, ID L2-L5 (2012)

8. Schlegel, E. M., A new subclass of Type II supernovae? *Mon. Not. R. Astron. Soc.*, **244**, 269-271 (1990)

9. Filippenko, A. V., Optical Spectra of Supernovae. *ARA&A*, **35**, 309-355 (1997)

10. Kiewe, M., Gal-Yam, A., Arcavi, I., et al., Caltech Core-Collapse Project (CCCP) Observations of Type IIn Supernovae: Typical Properties and Implications for Their Progenitor Stars. *Astrophys. J.*, **744**, 10 (2012)

11. Chugai, N. N., & Danziger, I. J., A Massive Circumstellar Envelope around the Type-IIn Supernova 1995G. *AstL*, **29**, 649-657 (2003)

12. Ofek, E. O., Cameron, P. B., Kasliwal, M. M., et al., SN 2006gy: An Extremely Luminous Supernova in the Galaxy NGC 1260. *Astrophys. J.*, **659**, L13-L16 (2007)

13. Smith, N., Li, W., Foley, R. J., et al., SN 2006gy: Discovery of the Most Luminous Supernova Ever Recorded, Powered by the Death of an Extremely Massive Star like η Carinae. *Astrophys. J.*, **666**, 1116-1128 (2007)

14. Owocki, S., Hot-Star Mass-Loss Mechanisms: Winds & Outbursts. *ASPC*, **425**, 199-208 (2010)

15. Smith, N., et al., Discovery of Precursor LBV Outbursts in Two Recent Optical Transients: The Fitfully Variable Missing Links UGC 2773-OT and SN 2009ip. *Astron. Jour.*, **139**, 1451–1467 (2010)

16. Pastorello, A., Botticella, M. T., Trundle, C., et al., Multiple major outbursts from a restless luminous blue variable in NGC 3432. *Mon. Not. R. Astron. Soc.*, **408**, 181-198 (2010)

17. Foley, R. J., Berger, E., Fox, O., et al., The Diversity of Massive Star Outbursts. I. Observations of SN 2009ip, UGC 2773 OT2009-1, and Their Progenitors. *Astrophys. J.*, **732**, 32 (2011)

18. Mauerhan, J. C., Smith, N., Filippenko, A. V., et al., The Unprecedented Third Outburst of SN 2009ip: A Luminous Blue Variable Becomes a Supernova. arXiv:1209.6320 (2012)

19. Prieto, J. L., Brimacombe, J., Drake, A. J., Howerton, S., The Rise of the Remarkable Type IIn Supernova SN 2009ip. arXiv:1210.3347 (2012)

20. Law, N. M., Kulkarni, S. R., Dekany, R. G., et al., The Palomar Transient Factory: System Overview, Performance, and First Results. *Pub. Astron. Soc. Pacific*, **121**, 1395-1408 (2009)

21. Rau, A., Kulkarni, S. R., Law, N. M., et al., Exploring the Optical Transient Sky with the Palomar Transient Factory. *Pub. Astron. Soc. Pacific*, **121**, 1334-1351 (2009)

22. Ofek, E. O., Laher, R., Law, N. M., et al., The Palomar Transient Factory Photometric Calibration. *Pub. Astron. Soc. Pacific*, **124**, 62-73 (2012)

23. Ofek, E. O., Laher, R., Surace, J., et al., The Palomar Transient Factory Photometric Catalog 1.0. *Pub. Astron. Soc. Pacific*, **124**, 854-860 (2012)

24. Ofek, E. O., Fox, D., Cenko, S. B., et al., X-ray emission from supernovae in dense circumstellar matter environments: A search for collisionless shocks. arXiv:1206.0748 (2012)

25. Taam, R. E., & Ricker, P. M., Common envelope evolution. *NewAR*, **54**, 65-71 (2010)

26. Rakavy, G., Shaviv, G., & Zinamon, Z., Carbon and Oxygen Burning Stars and Pre-Supernova Models *Astrophys. J.*, **150**, 131-162 (1967)

27. Quimby, R. M., Kulkarni, S. R., Kasliwal, M. M., et al., Hydrogen-poor superluminous stellar explosions. *Nature*, **474**, 487-489 (2011)

28. Ofek, E. O., et al., SN 2009ip: Constraints on the progenitor mass-loss rate. *submitted to ApJ*

29. Yaron, O., Gal-Yam, A., WISeREP - An Interactive Supernova Data Repository. *Pub. Astron. Soc. of the Pacific*, **124**, 668-681 (2012)

Supplementary Information is linked to the online version of the paper at www.nature.com/nature.

Acknowledgements

We thank Eliot Quataert and Matteo Cantiello for helpful discussions. The VLA is operated by the National Radio Astronomy Observatory, a facility of the U.S. National Science Foundation (NSF) operated under cooperative agreement by Associated Universities, Inc. This paper is based on observations obtained with the Samuel Oschin Telescope as part of the Palomar Transient Factory project. We are grateful for the assistance of the staffs at the various observatories where data were obtained. The authors acknowledge support from the Arye Dissentshik career development chair, the Helen Kimmel Center for Planetary Science, the Israeli Ministry of Science, the Royal Society, the NSF, the Israeli Science Foundation, the German-Israeli Foundation, ERC, the U.S. Department of Energy, Gary & Cynthia Bengier, the Richard & Rhoda Goldman Fund, the Christopher R. Redlich Fund, and the TABASGO Foundation.

Author contribution E. O. Ofek initiated the search for precursor outbursts and wrote the paper, M. Sullivan wrote the careful image-subtraction pipeline, S. B. Cenko reduced the *Swift*-UVOT observations, M. M. Kasliwal reduced the P60 observations, A. Gal-Yam helped with the the spectroscopic analysis, L. Bildsten, E. Nakar, and N. J. Shaviv contributed to the theoretical interpretation, A. V. Filippenko assisted with the spectroscopy and edited the paper, D. A. Howell, D. Murray, and J. M. Silverman conducted the spectroscopic observations or reductions, O. Yaron helped write the paper, and S. R. Kulkarni, I. Arcavi, J. S. Bloom, R. Laher, P. E. Nugent, and J. Surace built the PTF hardware and software infrastructure.

 Correspondence should be addressed to E. O. Ofek (e-mail: eran@astro.caltech.edu).

Figure 1: The light curve of SN 2010mc as obtained with the Palomar 48-inch telescope. The red circles are based on individual images, the squares are based on coadded images, while the empty triangles represent the 3σ upper limits derived from coadded images. The error bars represent the 1σ errors. The object magnitudes are given in the PTF magnitude system.[22],[23] Other datasets, including the Palomar 60-inch and *Swift*-UVOT, are listed in the SI (Table 3). All the photometric and spectroscopic data are available via the WISeREP website[29]. The dashed line shows the expected luminosity from the radioactive decay of an ejected mass of $0.1\,\mathrm{M}_\odot$ of Ni^{56}. Assuming that at late times the optical depth is sufficiently large to convert the radioactive energy to optical luminosity, but not too large so it will go into PdV work, this line represents an upper limit on the total amount of Ni^{56} in the ejecta; it was set to coincide with the latest observation of the SN at JD $\approx$ 2,455,758 (see Table 3). The dotted line represents a bolometric luminosity equal to 50 times the Eddington luminosity for a $50\,\mathrm{M}_\odot$ star (order of magnitude estimate of the mass of the progenitor assuming it is a massive star). The right edges of the "S" symbols above the light curve indicate the epochs at which we obtained spectra (see Fig. 2). A full version of this light curve, including the late-time observations, is shown in the SI.

Figure 2: Spectra of SN 2010mc, showing prominent Balmer emission lines. The early-time spectra are well fitted by a narrow component ($\sim 10^2\,\mathrm{km\,s^{-1}}$; the fit includes the instrumental line broadening) and a broad component extending to $\sim 3\times10^3\,\mathrm{km\,s^{-1}}$ at the first epoch, and decreasing to $10^3\,\mathrm{km\,s^{-1}}$ at the second epoch. At later epochs the Hα line develops a P-Cygni profile (similar to that of normal SNe II) with a velocity difference between the absorption bottom and the emission peak of $\sim 10^4\,\mathrm{km\,s^{-1}}$. At the first epochs we also detect He I lines, some of which are marked on the plot. They become weaker (see SI Figure 2) at later epochs, presumably due to the decrease in the effective temperature (see SI Figure 2). This, as well as the absence of He II lines, indicates that our temperature estimate (SI Figure 2) is reasonable.

Figure 3: Qualitative sketch of the proposed model for SN 2010mc. *Panel a*: At day ~ 0, an inner shell (purple) with a mass of $\sim 10^{-2}\,\mathrm{M}_\odot$, ejected about one month earlier, during the precursor outburst, and moving at about $2000\,\mathrm{km\,s^{-1}}$, is located at a radius of $\sim 7\times10^{14}\,\mathrm{cm}$. An outer shell (orange), found at a large radius and moving

at a few hundreds $\mathrm{km\,s^{-1}}$ (up to $10^3\,\mathrm{km\,s^{-1}}$), was ejected at earlier times. This indicates that the progenitor likely had multiple mass-loss episodes in the past tens to hundreds of years prior to the explosion. *Panel b*: At day ~ 5, the SN shock front (grey line) moving at $\sim 10^4\,\mathrm{km\,s^{-1}}$ is ionising the inner and outer shells which produce the broad and narrow Hα emission seen in the early-time spectra. *Panel c*: At day ~ 20, the SN shock engulfs the inner shell, and the intermediate width ($\sim 2000\,\mathrm{km\,s^{-1}}$) component of the H$\alpha$ line disappears. Instead we detect a $1000\,\mathrm{km\,s^{-1}}$ line, presumably due to material ejected during previous, but likely recent, mass-loss episodes and that is found at larger distances from the SN. We note that inspection of the SN light curve shows that around day 50 there is an indication for a possible rebrightening, perhaps resulting from the SN ejecta colliding with such additional material ejected at earlier times. At day ~ 20, the photospheric temperature decreases and it becomes optically thinner, and therefore we begin seeing an Hα P-Cygni profile with a velocity of $\sim 10^4\,\mathrm{km\,s^{-1}}$. This line become even stronger on day 27. This reflects the unshocked ejecta below the interaction zone.

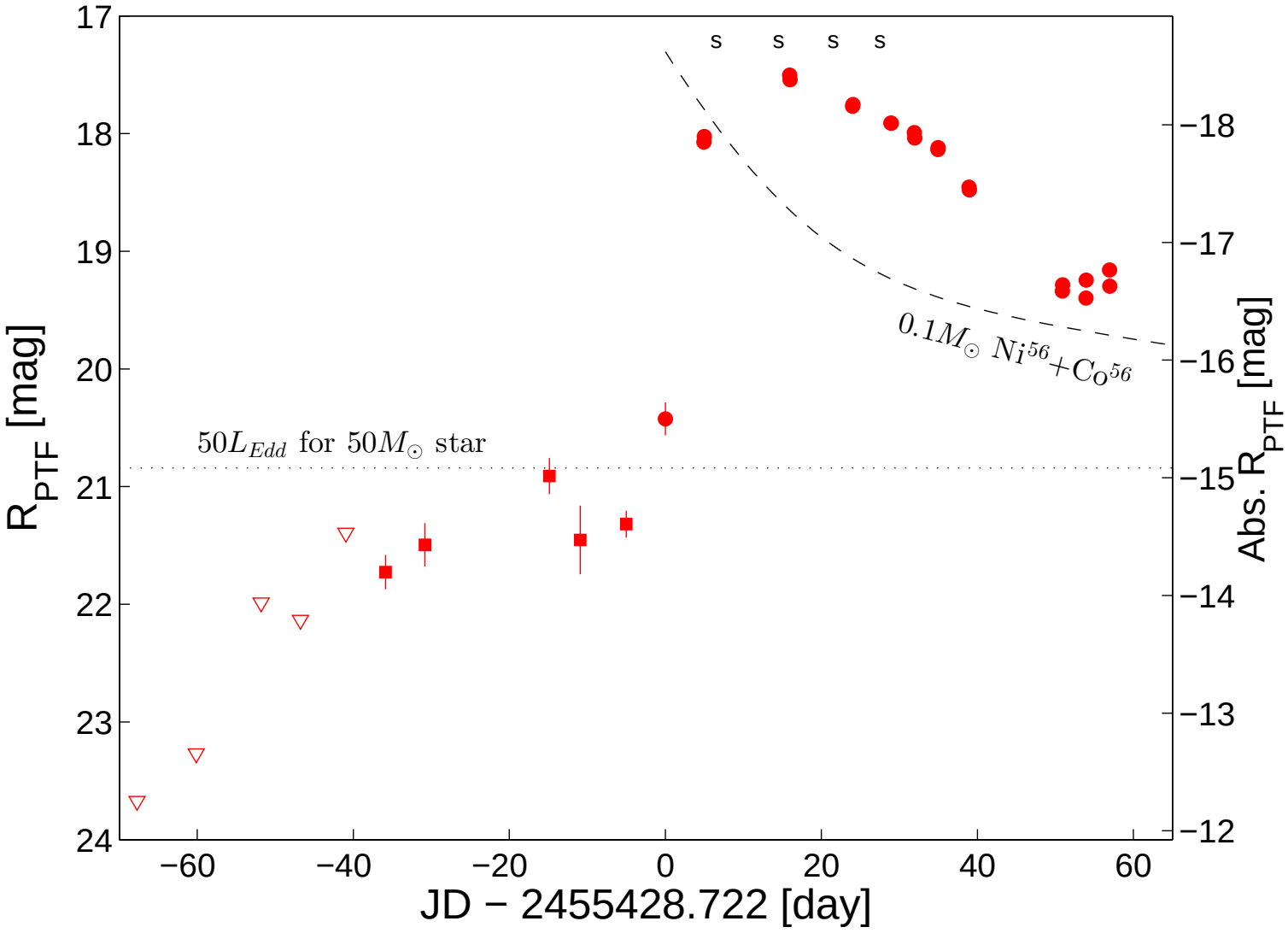
17
18
19
20
21
22
23
24
−18
−17
−16
−15
−14
−13
−12
−60
−40
−20
0
20
40
60
R_PTF [mag]
Abs. R_PTF [mag]
JD − 2455428.722 [day]
$50L_{Edd}$ for $50M_\odot$ star
$0.1M_\odot$ Ni^{56}+Co^{56}

Figure 1.

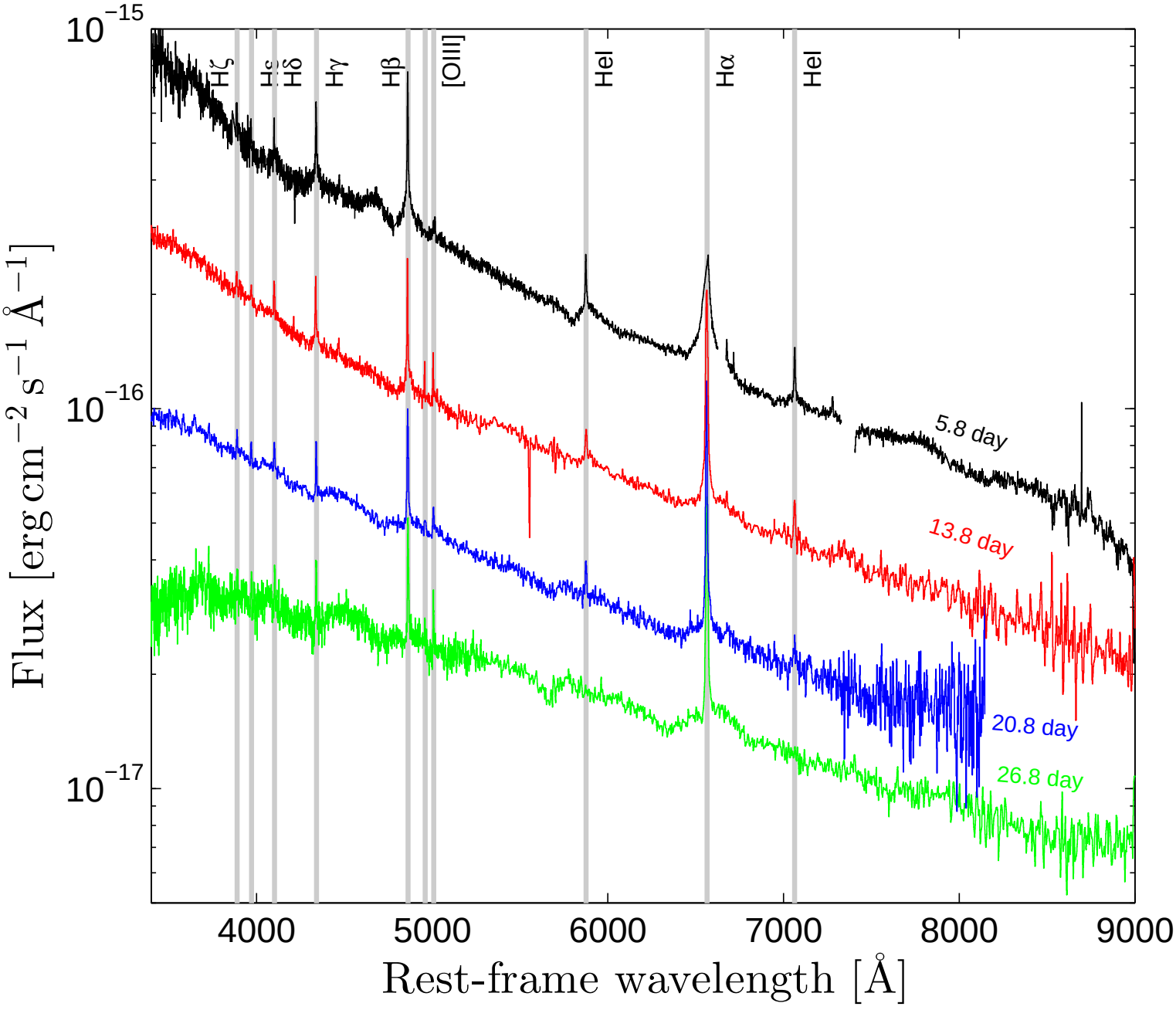
Hζ
Hε
Hδ
Hγ
Hβ
[OIII]
HeI
Hα
HeI
5.8 day
13.8 day
20.8 day
26.8 day
Flux [erg cm^{-2} s^{-1} Å^{-1}]
Rest-frame wavelength [Å]

Figure 2.

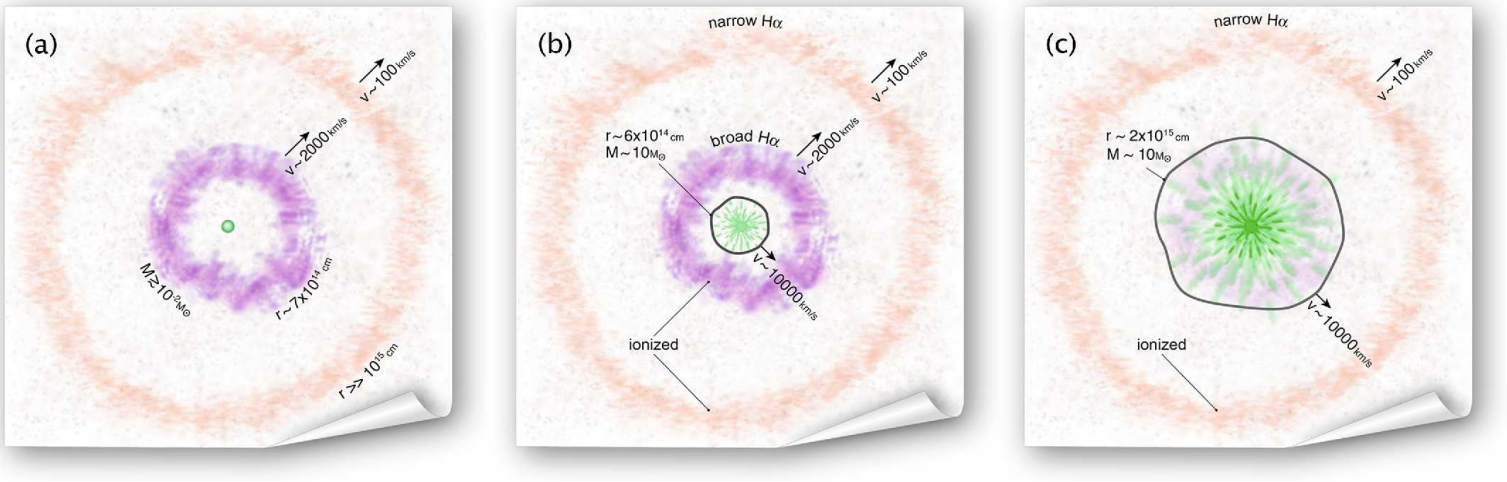

Figure 3.

SUPPLEMENTARY INFORMATION

1 Observations

1.1 Photometry and spectroscopy

On 2010 Aug. 25, the Palomar Transient Factory (PTF; Law et al. 2009; Rau et al. 2009) discovered with an autonomous machine-learning framework (Bloom et al. 2011) the Type IIn SN 2010mc (PTF 10tel; Ofek et al. 2012c) in images obtained on 2010 Aug. 20.22 UT. Further inspection of the images generated by the automatic image-subtraction pipeline revealed that the object was detected even on Aug. 20.22 (i.e., the discovery date).

We reanalysed the images using a careful image-subtraction pipeline. The improved reduction clearly shows a variable source at the location of the SN prior to the discovery date. Table 1 presents the photometric measurements of SN 2010mc, including observations made with the Oschin Schmidt 48-inch telescope, the Palomar 60-inch telescope (Cenko et al. 2006), and the *Swift*-UVOT (Gehrels et al. 2004). We note that the ground-based observations were processed using image subtraction.

A version of the light curve showing the late-time observations of the SN is presented in SI Figure 4.

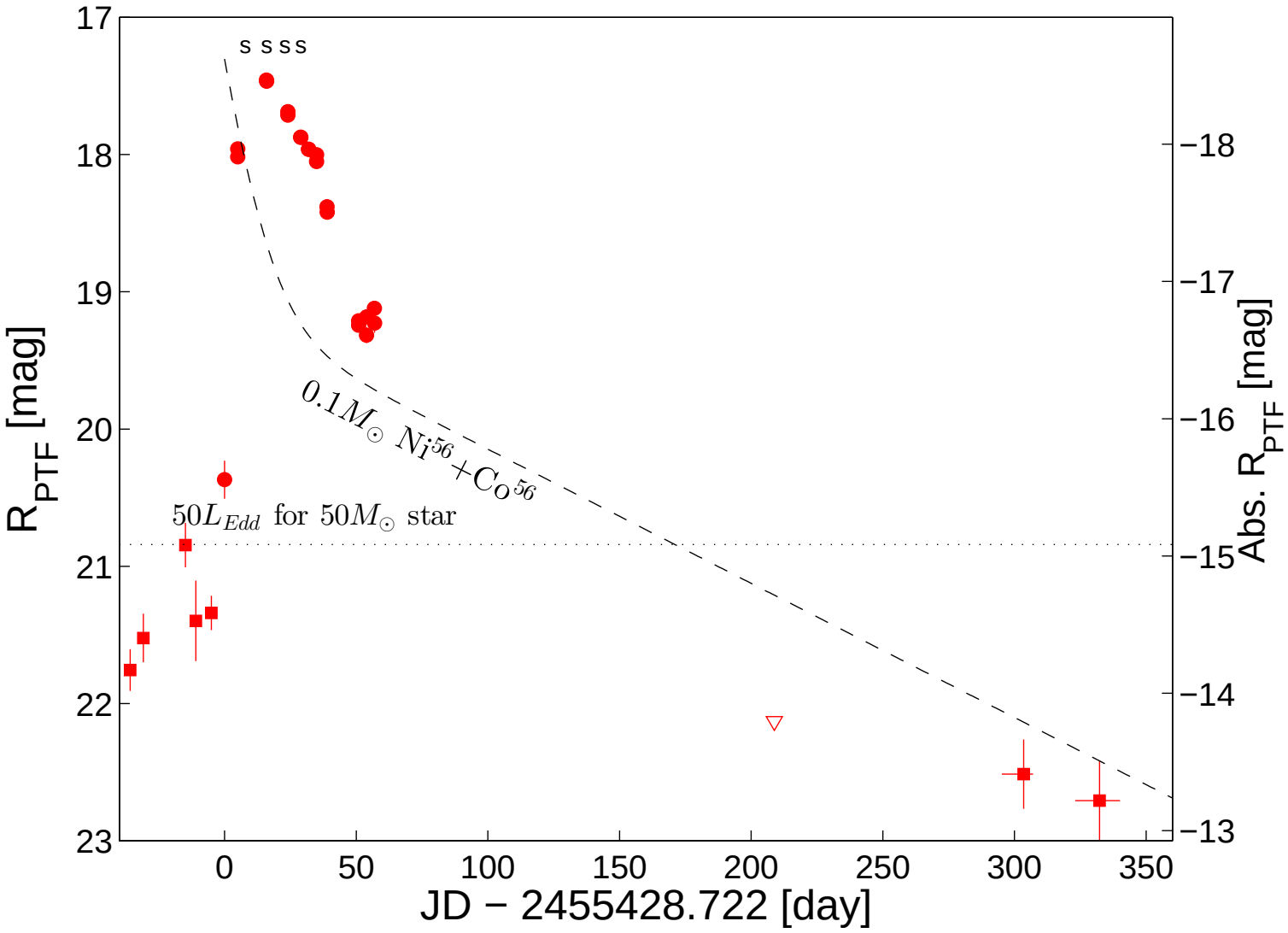

Figure 4. The light curve of SN 2010mc (PTF 10tel) as obtained with the Palomar 48-inch telescope, including late-time observations. See main text Figure 1 for details.

Telescope	Band	Time (day)	Δ_- (day)	Δ_+ (day)	N	AB Mag (mag)	Err (mag)	Mag limit (mag)
PTF	R	-0.0000	—	—	1	20.42	0.14	21.46
PTF	R	4.9600	—	—	1	18.07	0.02	21.34
PTF	R	5.0030	—	—	1	18.02	0.02	21.17
PTF	R	15.9350	—	—	1	17.50	0.01	21.05
PTF	R	15.9820	—	—	1	17.54	0.01	21.22
PTF	R	24.0140	—	—	1	17.77	0.01	21.32
PTF	R	24.0580	—	—	1	17.75	0.02	20.93
PTF	R	28.9200	—	—	1	17.91	0.01	21.54
PTF	R	28.9640	—	—	1	17.91	0.01	21.47
PTF	R	31.9190	—	—	1	17.99	0.02	21.42
PTF	R	31.9770	—	—	1	18.04	0.02	21.26
PTF	R	34.9320	—	—	1	18.14	0.02	21.43
PTF	R	34.9760	—	—	1	18.12	0.04	20.59
PTF	R	38.9240	—	—	1	18.45	0.03	21.20
PTF	R	38.9670	—	—	1	18.48	0.04	21.01
PTF	R	50.8910	—	—	1	19.34	0.03	22.07
PTF	R	50.9350	—	—	1	19.28	0.03	21.84
PTF	R	53.9120	—	—	1	19.40	0.06	21.39
PTF	R	53.9570	—	—	1	19.25	0.05	21.40
PTF	R	56.9350	—	—	1	19.16	0.04	21.58
PTF	R	56.9790	—	—	1	19.30	0.07	21.12
PTF	R	-35.8710	—	—	1	21.74	0.21	22.32
PTF	R	-35.8260	—	—	1	21.71	0.20	22.35
PTF	R	-30.8300	—	—	1	21.49	0.18	22.23
PTF	R	-14.8740	—	—	1	20.98	0.18	21.72
PTF	R	-5.0370	—	—	1	21.45	0.24	21.90
PTF	R	-4.9930	—	—	1	21.27	0.13	22.38
PTF	R	-35.8485	0.0225	0.0225	2	21.73	0.15	22.71
PTF	R	-30.8300	0.0000	0.0000	1	21.49	0.18	22.23
PTF	R	-14.8520	0.0220	0.0220	2	20.91	0.15	21.85
PTF	R	-10.9125	0.0225	0.0225	2	21.45	0.29	21.69
PTF	R	-5.0150	0.0220	0.0220	2	21.32	0.11	22.57
PTF	R	303.5230	8.3140	3.5980	5	22.44	0.23	22.93
PTF	R	332.5799	9.5219	7.5501	10	22.64	0.28	22.92
PTF	R	-125.7380	21.9790	11.0110	3	—	—	22.43
PTF	R	-96.3635	12.5635	13.5765	11	—	—	23.48
PTF	R	-70.3692	7.4648	8.5832	12	—	—	23.65
PTF	R	-67.7174	10.1166	15.9324	14	—	—	23.67
PTF	R	-60.1392	6.6858	8.3542	6	—	—	23.27
PTF	R	-51.8065	0.0215	0.0215	2	—	—	21.99
PTF	R	-51.8065	0.0215	0.0215	2	—	—	21.99
PTF	R	-46.7715	0.0225	0.0225	2	—	—	22.13
PTF	R	-40.9400	0.0000	0.0000	1	—	—	21.39
PTF	R	208.7957	1.5128	1.5122	4	—	—	22.19
PTF	R	355.6692	4.6512	6.3248	6	—	—	23.16
PTF	R	387.0123	4.0043	7.9167	3	—	—	22.48
PTF	R	419.9272	4.0323	4.0317	4	—	—	22.43

P60	g	5.9400	—	—	1	17.96	0.18	—
P60	g	7.9630	—	—	1	17.89	0.17	—
P60	g	10.0990	—	—	1	17.78	0.17	—
P60	g	10.1030	—	—	1	17.78	0.15	—
P60	g	14.0070	—	—	1	17.70	0.20	—
P60	g	15.0140	—	—	1	17.62	0.17	—
P60	g	16.0330	—	—	1	17.61	0.21	—
P60	g	17.0640	—	—	1	17.59	0.21	—
P60	g	18.0750	—	—	1	17.60	0.23	—
P60	g	19.0210	—	—	1	17.74	0.17	—
P60	g	20.0700	—	—	1	17.75	0.19	—
P60	g	21.9430	—	—	1	17.69	0.22	—
P60	g	23.0360	—	—	1	17.86	0.22	—
P60	g	32.0150	—	—	1	18.30	0.22	—
P60	g	34.9860	—	—	1	18.56	0.22	—
P60	g	40.9780	—	—	1	19.04	0.48	—
P60	g	49.9340	—	—	1	19.91	0.49	—
P60	g	50.9070	—	—	1	19.85	0.47	—
P60	g	51.9660	—	—	1	19.62	0.67	—
P60	g	52.9400	—	—	1	19.59	0.62	—
P60	g	53.9140	—	—	1	19.95	0.53	—
P60	g	55.9820	—	—	1	19.80	0.38	—
P60	g	56.9000	—	—	1	19.68	0.52	—
P60	g	69.9530	—	—	1	20.42	0.37	—
P60	g	72.8890	—	—	1	20.23	0.61	—
P60	r	7.9610	—	—	1	18.08	0.14	—
P60	r	10.0960	—	—	1	17.97	0.17	—
P60	r	10.1010	—	—	1	18.00	0.17	—
P60	r	14.0060	—	—	1	17.93	0.15	—
P60	r	15.0130	—	—	1	17.78	0.15	—
P60	r	16.0320	—	—	1	17.84	0.16	—
P60	r	17.0630	—	—	1	17.80	0.14	—
P60	r	18.0740	—	—	1	17.84	0.14	—
P60	r	19.0200	—	—	1	17.88	0.14	—
P60	r	20.0690	—	—	1	17.82	0.15	—
P60	r	21.9420	—	—	1	17.77	0.15	—
P60	r	23.0350	—	—	1	17.88	0.15	—
P60	r	32.0140	—	—	1	18.33	0.14	—
P60	r	34.0740	—	—	1	18.39	0.16	—
P60	r	49.9320	—	—	1	19.57	0.15	—
P60	r	51.9640	—	—	1	19.49	0.26	—
P60	r	53.9130	—	—	1	19.56	0.21	—
P60	r	55.9800	—	—	1	19.34	0.27	—
P60	r	72.8870	—	—	1	20.08	0.21	—
P60	i	7.9590	—	—	1	18.33	0.16	—
P60	i	10.0950	—	—	1	18.07	0.19	—
P60	i	10.1000	—	—	1	18.28	0.16	—
P60	i	14.0010	—	—	1	18.24	0.17	—
P60	i	15.0120	—	—	1	18.02	0.16	—
P60	i	16.0310	—	—	1	18.08	0.14	—
P60	i	17.0620	—	—	1	18.00	0.16	—

P60	i	18.0730	—	—	1	17.98	0.15	—
P60	i	19.0190	—	—	1	18.10	0.18	—
P60	i	20.0580	—	—	1	18.01	0.19	—
P60	i	21.9410	—	—	1	17.88	0.18	—
P60	i	23.0230	—	—	1	17.91	0.16	—
P60	i	32.0130	—	—	1	18.52	0.11	—
P60	i	34.0720	—	—	1	18.52	0.14	—
P60	i	49.9310	—	—	1	19.59	0.13	—
P60	i	53.9110	—	—	1	19.56	0.15	—
P60	i	55.9790	—	—	1	19.28	0.14	—
P60	i	68.9290	—	—	1	19.25	0.15	—
P60	i	74.9270	—	—	1	19.20	0.14	—
Swift/UVOT	UVW1	—	—	1	6.753	17.59	0.05	—
Swift/UVOT	UVW2	—	—	1	6.738	17.67	0.03	—
Swift/UVOT	UVW1	—	—	1	11.174	17.69	0.04	—
Swift/UVOT	UVW2	—	—	1	11.167	17.87	0.04	—
Swift/UVOT	UVW1	—	—	1	691.08	21.05	0.10	—
Swift/UVOT	U	—	—	1	691.88	20.54	0.08	—

Table 1: SN 2010mc (PTF 10tel) photometric measurements. Time is measured relative to JD = 2,455,428.722 day. Δ_- and Δ_+ are the lower and upper time range in which the photometry was obtained. These columns are indicated in cases where we coadded data from several images. N is the number of images. PTF magnitudes are given in the PTF magnitude system (Ofek et al. 2012a; Ofek et al. 2012b). The *Swift*/UVOT measurements represents the aperture magnitude at the position of the SN and include the host-galaxy light. The two last UVOT measurements were taken at late times; thus, they can be regarded as the magnitudes of the host galaxy. Based on them, we conclude that in order to correct the early-time measurements for the host-galaxy contamination, about 0.05 mag should be added to the SN magnitudes.

UT Date	Telescope	Instrument	Hα flux ($\mathrm{erg\,cm^{-2}\,s^{-1}}$)	broad Hα vel. ($\mathrm{km\,s^{-1}}$)	narrow Hα vel. ($\mathrm{km\,s^{-1}}$)
2010 Aug. 26	Gemini	GMOS	9.2×10^{-15}	3400	800
2010 Sep. 03	Lick	Kast	1.2×10^{-14}	1100	160
2010 Sep. 10	KPNO	RC spectrograph	9.2×10^{-15}	670	110
2010 Sep. 16	Lick	Kast	1.4×10^{-14}	4000	230

Table 2. Log of spectroscopic observations of SN 2010mc (PTF 10tel) and properties of the Hα emission line. The fluxes and velocities were measured by fitting two-component Gaussians which were convolved with the instrumental broadening as estimated from atmospheric emission lines.

In addition, we obtained spectra of SN 2010mc on four epochs, as listed in Table 2 and presented in Figure 2 of the main paper and SI Figure 5. In order to measure the line fluxes in a consistent way, we first calibrated the flux of each spectrum such that the synthetic $R_{\rm PTF}$ magnitude derived from the spectrum was identical to the $R_{\rm PTF}$ magnitude, interpolated to the epoch of each spectrum, from the PTF magnitudes listed in Table 1. All of the spectra are available online from the WISeREP website* (Yaron & Gal-Yam 2012). Each spectrum was smoothed using a median filter and a black-body curve was fitted. The derived effective temperatures and radii are presented in SI Figure 6.

The X-ray observations of PTF 10tel are presented and discussed in Section 3.

2 Derivation of mass loss as a function of the Hα line luminosity

Here we derive a relation between the mass in the circumstellar matter (CSM), the Hα emission-line luminosity $L_{\rm H\alpha}$, and the radius r. We assume that the CSM has a wind-density profile of the form $\rho = Kr^{-2}$, where $K \equiv \dot{M}/(4\pi v_{\rm w})$, $\dot{M}$ is the mass-loss rate, and $v_{\rm w}$ is the wind/outburst velocity. In this case the particle density profile is given by (e.g., Ofek et al. 2012c)

$$\begin{aligned} n &\approx \frac{1}{\langle\mu_{\rm p}\rangle}\frac{\dot{M}}{4\pi m_{\rm p} v_{\rm w} r^2} \\ &\approx 3.02\times10^{11}\frac{1}{\langle\mu_{\rm p}\rangle}\frac{\dot{M}}{0.1\,{\rm M_\odot\,yr^{-1}}}\left(\frac{v_{\rm w}}{10\,{\rm km\,s^{-1}}}\right)^{-1}\left(\frac{r}{10^{15}\,{\rm cm}}\right)^{-2}{\rm cm^{-3}}, \end{aligned} \quad (1)$$

*http://www.weizmann.ac.il/astrophysics/wiserep/; Weizmann Interactive Supernova (data) REPository.

where $\langle \mu_{\rm p} \rangle$ is the mean number of nucleons per particle (mean molecular weight). For our order-of-magnitude calculation, we adopt $\langle \mu_{\rm p} \rangle = 0.6$. Assuming the SN radiation field can ionise all of the hydrogen in the CSM, the mass of the hydrogen generating the Hα line is

$$M_{\rm H} \approx \frac{m_{\rm p} L_{\rm H\alpha}}{h \nu_{\rm H\alpha} \alpha^{\rm eff}_{\rm H\alpha} n_{\rm e}}. \quad (2)$$

Here $\nu_{\rm H\alpha}$ is the Hα frequency ($4.57 \times 10^{14}\,{\rm Hz}$), $\alpha^{\rm eff}_{\rm H\alpha}$ is the Hα effective recombination coefficient, $\sim 8.7 \times 10^{-14} T_{\rm 10k}^{-0.89}\,{\rm cm^3\,s^{-1}}$ (Osterbrock & Ferland 2006), where $T_{\rm 10k}$ is the temperature in units of 10,000 K. We assume $T_{\rm 10k} = 1$. In a wind profile, the integrated mass from radius r_0 to r is

$$M = \int_{r_0}^{r} 4\pi r^2 K r^{-2} dr = 4\pi K (r - r_0) \approx 4\pi K r, \quad (3)$$

where the last step assumes that $r_0 \ll r$. By substituting Equation 1 into Equation 2 and setting it equal to Equation 3, we can get a relation between the mass-loading parameter K, the Hα luminosity, and the radius:

$$\begin{aligned} K &\gtrsim \Big(\frac{\langle \mu_{\rm p} \rangle m_{\rm p}^2 L_{\rm H\alpha} r}{4\pi h \nu \alpha^{\rm eff}}\Big)^{1/2} \\ &\approx 7.1 \times 10^{15} \Big(\frac{L_{\rm H\alpha}}{10^{41}\,{\rm erg\,s^{-1}}}\Big)^{1/2} \Big(\frac{r}{10^{15}\,{\rm cm}}\Big)^{1/2} {\rm g\,cm^{-1}}. \end{aligned} \quad (4)$$

The reason for the inequality is that in practice, it is possible that not all of the hydrogen is ionised or that the temperature of the gas is too high (i.e., $\alpha^{\rm eff}_{\rm H\alpha}$ depends on temperature).

Assuming the outburst ejected material with a velocity of $2000\,{\rm km\,s^{-1}}$ at day -37, then at the time the first spectrum was taken (day 6), the ejecta radius is $r \approx 7 \times 10^{14}$ cm. This radius is consistent with the one derived from the black-body fit to the spectrum at the first epoch (see SI Figure 6). Using the measured flux of the Hα broad component at day 6 ($9 \times 10^{-15}\,{\rm erg\,cm^{-2}\,s^{-1}}$; Table 2), the luminosity of the Hα broad component is $\sim 3 \times 10^{40}\,{\rm erg\,s^{-1}}$. Substituting these values into Equation 4, and assuming a wind velocity of $2000\,{\rm km\,s^{-1}}$, we find a mass-loss rate of $\gtrsim 10^{-1}\,{\rm M_\odot\,yr^{-1}}$. Assuming a one month long outburst this gives a total mass of about $10^{-2}\,{\rm M_\odot}$. This value is in excellent agreement with the mass-loss rate we independently find based on the kinetic-energy arguments and the diffusion time scale.

We note that this derivation assumes that the narrow lines are due to the interaction of the CSM with the SN radiation field. One caveat, is that it is possible that some, or all,

UT Date	Time since disc. (day)	Exp. Time (s)	2σ upper limit ($\mathrm{ct\,ks^{-1}}$)
2010 Aug. 27.0	6.8	1342	2.2
2010 Aug. 31.4	11.2	2256	1.3
2012 July 11.7	691.5	4818	0.62

Table 3. *Swift*-XRT observations of SN 2010mc (PTF 10tel).

of the line flux originates from a shock interaction or from a slow moving ejecta. However, the order of magnitude consistency between this mass-loss estimate and other mass-loss estimators suggest that such an effect is not significant.

3 X-ray observations

The *Swift*-XRT observations of SN 2010mc (PTF 10tel) in the 0.2–10 keV band are listed in Table 3. For each *Swift*-XRT image of the SN, we extracted the number of X-ray counts in the 0.2–10 keV band within an aperture of 7.2″ (3 pixels) radius centred on the SN position. We chose a small aperture in order to minimise any host-galaxy contamination. We note that this aperture contains $\sim 37\%$ of the source flux (Moretti et al. 2004). The background count rates were estimated in annuli around each SN, with an inner (outer) radius of 50″ (100″). Assuming a photon spectrum $n_{\rm ph} \propto E^{-\Gamma}$ with $\Gamma = 2$, a Galactic neutral hydrogen column density of $2.34 \times 10^{20}\,\mathrm{cm^{-2}}$ in the direction of the SN (Dickey & Lockman 1990), and correcting for the photometric aperture losses, we find a 2σ upper limit on the luminosity in the second epoch of $3.5 \times 10^{41}\,\mathrm{erg\,s^{-1}}$.

Following Immler et al. (2008), the X-ray emission from the optically thin region is given by

$$L_{\rm X} \approx \int_r^{\infty} 4\pi r^2 \Lambda(T) n^2 dr, \qquad (5)$$

where $\Lambda(T)$ is the effective cooling function in the 0.2–10 keV range. Assuming an optically thin thermal plasma with a temperature in the range 10^6–10^8 K (Raymond et al. 1976), we adopt a value of $\Lambda(T) \approx 3 \times 10^{-23}\,\mathrm{erg\,cm^3\,s^{-1}}$. Substituting Equation 1 into Equation 5 we get

$$L_{\rm X} \approx 4\pi\Lambda(T)\frac{K^2}{\langle\mu_{\rm p}\rangle^2 m_{\rm p}^2 r}$$

$$\approx \quad 2.4\times10^{40}\Big(\frac{\dot{M}}{0.01\,\mathrm{M_\odot\,yr^{-1}}}\Big)^{2}\Big(\frac{v_w}{2000\,\mathrm{km\,s^{-1}}}\Big)^{-2}\Big(\frac{r}{10^{15}\,\mathrm{cm}}\Big)^{-1}\mathrm{e}^{-(\tau+\tau_{\rm bf})}\,\mathrm{erg\,s^{-1}}. \quad (6)$$

Here, we added a correction factor due to absorption in the wind, where τ and $\tau_{\rm bf}$ are the Thomson and bound-free optical depths, respectively. In our case the Thomson optical depth will be 1 for $\dot{M}\approx0.1\,\mathrm{M_\odot\,yr^{-1}}$ (e.g., Ofek et al. 2012c). Although the Thomson optical depth is well known, when the optical depth is of the order of a few, Compton scattering is expected to reprocess more energetic photons into the 0.2–10 keV band (Chevalier & Irwin 2012; Svirski et al. 2012). Since the exact X-ray spectrum is not known (Katz et al. 2011; Svirski et al. 2012), a proper calculation of $L_{\rm X}$ when $\tau\gtrsim1$ is not straightforward. Regarding the bound-free optical depth, although it is likely that all the hydrogen is ionised, Chevalier & Irwin (2012) argued that if the shock velocity is below $\sim10^4\,\mathrm{km\,s^{-1}}$ some of the metals will be neutral. In this case bound-free absorption will be important and it is given by (Ofek et al. 2012c)

$$\tau_{\rm bf}\approx15\Big(\frac{\dot{M}}{0.01\,\mathrm{M_\odot\,yr^{-1}}}\Big)\Big(\frac{v_{\rm w}}{2000\,\mathrm{km\,s^{-1}}}\Big)^{-1}\Big(\frac{r}{10^{15}\,\mathrm{cm}}\Big)^{-1}\Big(\frac{E_{\rm X}}{1\,\mathrm{keV}}\Big)^{-2.5}, \quad (7)$$

where $E_{\rm X}$ is the X-ray energy.

If we ignore the Thomson optical depth (i.e., $\tau=0$), and if we assume a flat spectrum (i.e., constant number of photons per unit energy) and the *Swift*-XRT spectral response, from Equations 6 and 7 we find that the mass-loss rate is either smaller than about $0.1\,\mathrm{M_\odot\,yr^{-1}}$ or larger than about $1\,\mathrm{M_\odot\,yr^{-1}}$. The low bound of $\dot{M}\lesssim0.1\,\mathrm{M_\odot\,yr^{-1}}$ is consistent with the other mass-loss estimates.

4 Radio observations

We observed SN 2010mc (PTF 10tel) with the Jansky Very Large Array (JVLA[†]) on 2012 Sep. 10, about two years after the SN discovery. The observation was undertaken in the K band (21.8 GHz). We used J1727+4530 for phase calibration and 3C 286 for flux calibration. The data were reduced using the AIPS software. We did not detect SN 2010mc with an upper limit of 0.2 mJy (3σ).

[†]The Jansky Very Large Array is operated by the National Radio Astronomy Observatory (NRAO), a facility of the National Science Foundation operated under cooperative agreement by Associated Universities, Inc.

5 Diffusion time scale limit on mass loss

Another observable that can be used to constrain the mass in the CSM is the rise time of the SN light curve. If a considerable amount of material is present between the SN and the observer, then photon diffusion will slow down the rise time of the SN light curve. Therefore, the maximum observed SN rise time can be used to put an upper limit on the amount of mass between the SN and the observer. The diffusion time scale in a wind profile is given by (e.g., Ginzburg et al. 2012)

$$\begin{aligned} t_{\rm diff} &\approx \frac{\kappa K}{c}[\ln\left(\frac{c}{v_{\rm sh}}\right)-1] \\ &\approx 0.08\left(\frac{\kappa}{0.34\,{\rm cm^2\,gr^{-1}}}\right)\left(\frac{\dot{M}}{10^{-2}\,{\rm M_\odot\,yr^{-1}}}\right)\left(\frac{v_{\rm w}}{2000}\right)^{-1}\left[\ln\left(30\frac{v_{\rm ej}}{10^4\,{\rm km\,s^{-1}}}\right)-1\right]\,{\rm day} \end{aligned} \quad (8)$$

Here $v_{\rm ej}$ is the SN shock velocity. In our case, assuming the rise time of the SN is about seven days, we can use Equation 8 to set an upper limit, $\dot{M} < 0.4\,{\rm M_\odot\,yr^{-1}}$.

6 Alternative interpretations

Here we consider alternative interpretations regarding the nature of the precursor bump and show that they are not consistent with the observations. One possibility is that this feature is due to a shock breakout (e.g., Colgate 1974) prior to the SN rise. However, given the feature's luminosity, its duration is at least an order of magnitude too long to be consistent with a shock breakout (e.g., Nakar & Sari 2010; Rabinak & Waxman 2011).

A second possibility is that the first bump represents a SN explosion while the second peak is due to the interaction of the SN ejecta with dense CSM and the conversion of the SN kinetic energy into radiated luminosity. However, this scenario can be rejected based on the fact that by fitting a black-body spectrum to the spectra (see SI Figure 6), we can find the temperature and photospheric radius evolution between days 5 and 27. These fits suggest that the photosphere is expanding with a mean velocity of $\gtrsim 4300\,{\rm km\,s^{-1}}$, and that the black-body radius at day 6 is $\sim 6\times10^{14}\,{\rm cm}$. Extrapolating backward, this suggests that the SN outburst happened after day -10.

Another argument against this scenario is that the SN spectrum at day 27 after discovery (main text Figure 2), shows a P-Cygni profile with a velocity of $\sim 10^4\,{\rm km\,s^{-1}}$. At the same time, the black-body radius of the SN photosphere is $\sim 1.5\times10^{15}\,{\rm cm}$. These values

are roughly consistent (to within 30%) with an explosion time at day 0, and are less consistent with explosion at day −37 day relative to discovery. A caveat in this statement is that the photospheric radius which controls the black-body temperature of the continuum is not necessarily at the same position where the P-Cygni absorption is generated.

7 The Type Ibn SN 2006jc

Another possibly related event is SN 2006jc (Nakano et al. 2006). Unlike SN 2010mc (PTF 10tel) and SN 2009ip, this was a hydrogen-stripped Type Ibn SN. In this case an optical outburst was observed in 2004, about two years prior to the SN explosion (Nakano et al. 2006), creating a dense circumstellar shell (Foley et al. 2007; Immler et al. 2008; Smith et al. 2008; Ofek et al. 2012c). Foley et al. (2007) suggested that the progenitor was a Wolf-Rayet star that had an outburst two years prior to its explosion, creating the CSM; it may have recently transitioned from the LBV phase. However, Pastorello et al. (2007) argued that SN 2006jc took place in a binary system in which one star (a Wolf-Rayet star) was responsible for the SN explosion while the companion was a luminous blue variable (LBV) that generated the eruption in 2004. Our argument regarding the causality between pre-explosion outbursts and the SN explosions disfavours the explanation given by Pastorello et al. (2007) for SN 2006jc. However, for SN 2006jc, the time difference between the precursor event and the explosion is about two years (rather than one month), rendering the argument a factor ~ 20 weaker than in the case of PTF 10tel.

8 The probability of detecting a precursor outburst prior to the explosion

The specific precursor event reported in this paper was found as a part of a search for outbursts among type-IIn SN in PTF data. The sample we used included only four nearby type-IIn SNe with good pre-explosion coverage. Nevertheless, in estimating the probability of detecting a precursor prior to the explosion we assumed a sample size of 20 (five times higher than our actual sample size), accounting for other samples in which outburst events could have been detected (see details below). This sample size thus facilitates a conservative rate estimate.

Thus far the brightest precursor outbursts (e.g., PTF 10tel) have an absolute magnitude

of about -16. Using previous-generation transient surveys, such bursts can be detected up to a distance of ~ 100 Mpc, while the new-generation surveys (e.g., PTF) may be able to detect them to somewhat larger distances. Among the 165 SNe IIn listed in the IAUC website, about 70 have distances below 100 Mpc. Many of these SNe were found using small telescopes which are limited by their depth. Based on the PTF experience, we estimate that not more than 20% of these SNe have sufficiently good pre-explosion observations that will allow the detection of a precursor prior to the explosion. In addition, PTF has already found 91 SNe IIn (some listed in the IAUC website), of which only a few are sufficiently nearby, and have high cadence and almost continuous observations prior to the explosion. Thus, we conclude that up to 20 SNe IIn discovered so far have good enough pre-explosion observations to find precursor outbursts.

We note that even if we assume that *all* of the ~ 250 SNe IIn discovered so far have sufficiently good observations prior to the SN explosion, this will not change our conclusion that precursor outbursts are more common, or are causally connected with the final stages of massive-star evolution.

Finally, we note that we cannot completely rule out the possibility that the SN and precursor are two unrelated events (e.g., explosions of two different stars in a star cluster). However, we think this is an unlikely possibility given the evidences presented in this paper, including consistency of the mass-loss estimators with the properties of the outburst (luminosity and time before SN), and the small number of type-IIn SNe in which we searched for precursor events.

9 Theoretical determination of the precursor mass loss

The precursor is characterised by a rapid brightening of the radiative flux which is sustained at a highly super-Eddington level for a month. The relatively short time scales imply that some efficient mechanism exists to very quickly transport the flux out, even faster than convection can. The mechanism suggested by Quataert & Shiode (2012), where the energy is transported outward by acoustic waves, offers a natural explanation. However, this mechanism can operate only in regions with a sufficiently high density. At a region where the density, ρ, satisfies $L \approx L_{\rm conv,max} \approx 4\pi r^2 \rho v_{\rm s}^3$ (where $v_{\rm s}$ is the speed of sound), the

acoustic energy flux L is converted into a radiative flux L. The mass-loss rate expected in such a case is $\dot{M} \approx 4\pi r^2 \rho v_\mathrm{s} \approx L/v_\mathrm{s}^2$. Assuming $v_\mathrm{s} \approx 60\,\mathrm{km\,s^{-1}}$ at the base of the wind gives roughly $8\,\mathrm{M}_\odot$ for the mass ejected during the precursor. A similar problem exists for the great (super-Eddington) eruption of η Carina. The naive expectation for the mass loss is orders of magnitude larger than what was actually observed (Shaviv 2000).

To overcome this discrepancy, it was suggested that instabilities reduce the effective opacity of super-Eddington atmospheres. This implies that a wind is accelerated only from lower-density regions where a typical scale height in the atmosphere becomes of order unity and the effective opacity returns to its microscopic value. Under these assumptions, the mass-loss was determined by Shaviv (2001) to be $\Delta M = W \Delta T (L - L_\mathrm{Edd})/(c v_\mathrm{s})$, where ΔT is the duration of the outburst and L is the luminosity at the base of the wind (where part of the latter is converted into mechanical energy of the mass loss). W is a dimensionless constant which depends on the geometry of the instabilities, and empirically was found to be around 3 (± 0.5 dex).

We can use this expression to predict the expected mass loss from the super-Eddington precursor. To do so we have to add the mechanical energy of the wind to the observed luminosity and obtain the total luminosity at the base of the wind. The mechanical energy itself is given by $L_\mathrm{mech} = \Delta M/2(v_\infty^2 + v_\mathrm{esc}^2)$. Here v_∞ is the terminal velocity at infinity and v_esc is the escape velocity. We crudely take $v_\mathrm{esc} \approx v_\infty$. Since the luminosity at the base is significantly super-Eddington, we can ignore the L_Edd term. If we further consider that $v_\mathrm{s} \approx 30\,\mathrm{km\,s^{-1}}$, we obtain $\Delta M \approx 0.05\,\mathrm{M}_\odot$ (with an uncertainty of about 0.5 dex). This value sits comfortably in the observationally determined range of possible mass loss in SN 2010mc (PTF 10tel).

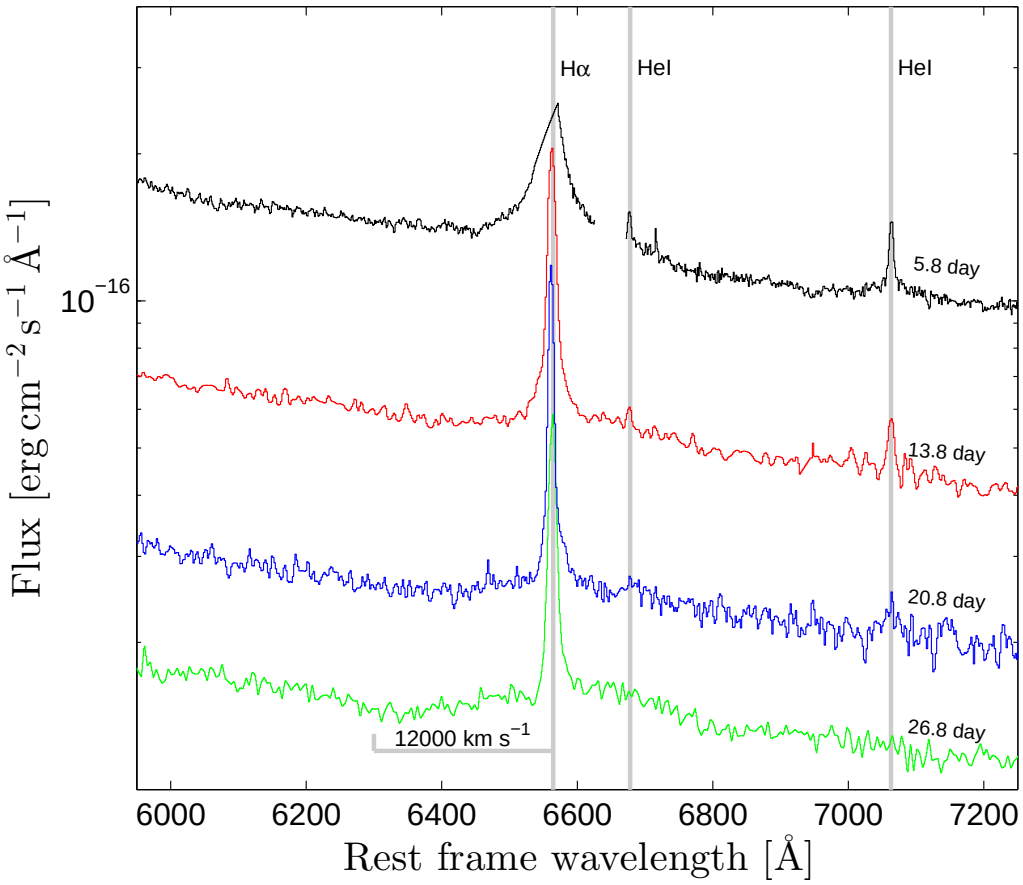

Figure 5. Close-up view of the Hα line in the spectra of SN 2010mc (PTF 10tel). The best–fit width and total flux of a two-component model at each epoch are listed in Table 2. The width of the Hα emission is decreasing significantly after the first epoch, from 3400 km s^{-1} to $\lesssim$ 1000 km s^{-1}. In the last epoch a P-Cygni profile develops, with a velocity difference between the peak of the emission and the bottom of the absorption of over 10^4 km s^{-1}. The velocity of the Hα absorption component in the P-Cygni feature is marked with a 12,000 km s^{-1} label. The P-Cygni profile is better seen in the stretch of Figure 2 (main text). Also visible is the decrease in strength of the He I lines, presumably due to the decrease in temperature (see SI Figure 6).

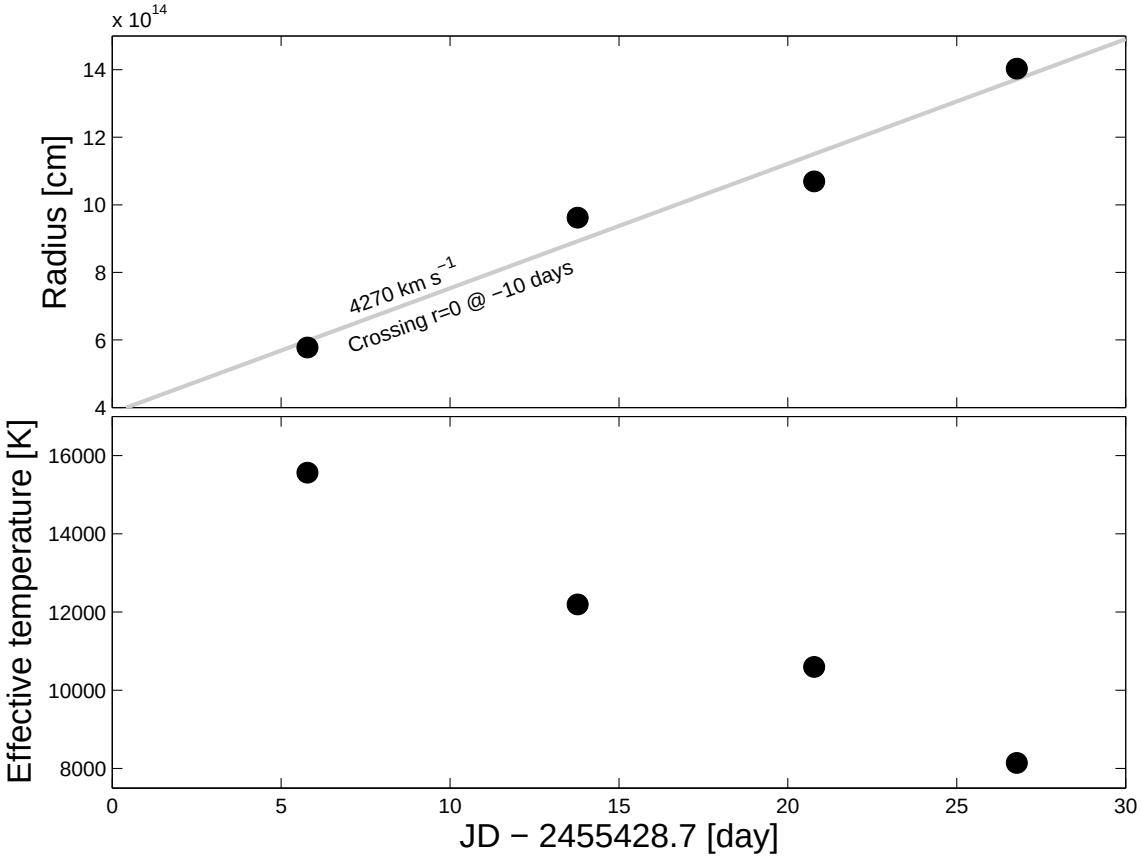

Figure 6. Black-body temperature and radius derived from the spectra of SN 2010mc (PTF 10tel). The temperature estimate should be regarded as a lower limit, because the peak of the emission is outside the optical region and metal line blanketing can reduce the flux in the blue parts of the spectrum. The reduction in temperature is consistent with the fact that the He I lines are becoming weaker at later epochs (SI Figure 5). We note that the best-fit temperature at day 6 (near the first spectroscopic observation) based on the broad-band *Swift*/UVOT and P60 photometry is about 19,000 K. The nondetection of He II lines also suggests that the temperature is not much higher than the value derived here.

Received 13 February 2013; Accepted **draft**.

30. Bloom, J. S., Richards, J. W., Nugent, P. E., et al., Automating Discovery and Classification of Transients and Variable Stars in the Synoptic Survey Era. arXiv:1106.5491 2011

31. Cenko, S. B., Fox, D. B., Dae-Sik, M., et al., The Automated Palomar 60 Inch Telescope. *PASP*, **118**, 1396-1406 (2006)

32. Chevalier, R. A., Irwin, C. M., X-Rays from Supernova Shocks in Dense Mass Loss. *ApJ*, **747**, L17 (2012)

33. Dickey, J. M., Lockman, F. J., H I in the Galaxy. *ARA&A*, 215-261 (1990)

34. Colgate, S. A., Early Gamma Rays from Supernovae. *ApJ*, **187**, 333-336 (1974)

35. Foley, R. J., Smith, N., Ganeshalingam, M., et al., SN 2006jc: A Wolf-Rayet Star Exploding in a Dense He-rich Circumstellar Medium. *ApJ*, **657**, L105-108 (2007)

36. Gehrels, N., Chincarini, G., Giommi, P., et al., The Swift Gamma-Ray Burst Mission. *ApJ*, **611**, 1005-1020 (2004)

37. Immler, S., Modjaz, M., Landsman, W., et al., Swift and Chandra Detections of Supernova 2006jc: Evidence for Interaction of the Supernova Shock with a Circumstellar Shell. *ApJ*, **674**, L85-88 (2008)

38. Katz, B., Sapir, N., Waxman, E., X-rays, gamma-rays and neutrinos from collisionless shocks in supernova wind breakouts. arXiv 1106.1898

39. Nakar, E., Sari, R., Early Supernovae Light Curves Following the Shock Breakout. *ApJ*, **725**, 904-921 (2010)

40. Quataert, E., & Shiode, J. Astrophysics of gaseous nebulae and active galactic nuclei, 2nd. ed

41. Raymond, J. C., Cox, D. P., Smith, B. W., et al., Radiative cooling of a low-density plasma. *ApJ*, **204**, 290-292 (1976)

42. Shaviv, N. J., The Porous Atmosphere of η Carinae. *ApJ*, **532**, L137-140 (2000)

43. Shaviv, N. J., The theory of steady-state super-Eddington winds and its application to novae. *MNRAS*, **326**, 126-146 (2001)

44. Svirski, G., Nakar, E., Sari, R., Optical to X-rays SNe light curves following shock breakout through a thick wind. arXiv 1202.3437

45. Rabinak, I., Waxman, E., The Early UV/Optical Emission from Core-collapse Supernovae. *ApJ*, **728**, 63 (2011)

46. Ginzburg, S., Balberg, S. Superluminous Light Curves from Supernovae Exploding in a Dense Wind. *ApJ*, **757**, 178-191 (2012)